Chapter 1

Design Techniques for Conformal Microstrip Antennas and Their Arrays

Daniel B. Ferreira, Cristiano B. de Paula and
Daniel C. Nascimento

Additional information is available at the end of the chapter

http://dx.doi.org/10.5772/53019

1. Introduction

Owing to their electrical and mechanical attractive characteristics, conformal microstrip antennas and their arrays are suitable for installation in a wide variety of structures such as aircrafts, missiles, satellites, ships, vehicles, base stations, etc. Specifically, these radiators can become integrated with the structures where they are mounted on and, consequently, do not cause extra drag and are less visible to the human eye; moreover they are low-weight, easy to fabricate and can be integrated with microwave and millimetre-wave circuits [1,2]. Nonetheless, there are few algorithms available in the literature to assist their design. The purpose of this chapter is to present accurate design techniques for conformal microstrip antennas and arrays composed of these radiators that can bring, among other things, significant reductions in design time.

The development of efficient design techniques for conformal microstrip radiators, assisted by state-of-the-art computational electromagnetic tools, is desirable in order to establish clear procedures that bring about reductions in computational time, along with high accuracy results. Nowadays, the commercial availability of high performance three-dimensional electromagnetic tools allows computer-aided analysis and optimization that replace the design process based on iterative experimental modification of the initial prototype. Software such as CST®, which uses the Finite Integration Technique (FIT), and HFSS®, based on the Finite Element Method (FEM), are two examples of analysis tools available in the market [3]. But, since they are only capable of performing the analysis of the structures, the synthesis of an antenna needs to be guided by an algorithm whereby iterative

process of simulations, result analysis and model's parameters modification are conducted until a set of goals is satisfied [4].

Generally, the design of a probe-fed microstrip antenna starts from an initial geometry determined by means of an approximate method such as the Transmission-line Model [5-7] or the Cavity Model [8]. Despite their numerical efficiency, i.e., they are not time-consuming and do not require a powerful computer to run on, these methods are not accurate enough for the design of probe-fed conformal microstrip antennas, leading to the need of antenna model optimization through the use of full-wave electromagnetic solvers in an iterative process. However, the full-wave simulations demand high computational efforts. Therefore, it is advantageous to have a design technique that employs full-wave electromagnetic solvers for accuracy purposes, but requires a small number of simulations to accomplish the design. Unfortunately, the approximated methods mentioned before provide no means for using the full-wave solution data in a feedback scheme, what precludes their integration in an iterative design process, hence restricting them just to the initial design step. In this chapter, in order to overcome this drawback and to reduce the number of full-wave simulations required to synthesize a probe-fed conformal microstrip antenna with quasi-rectangular patch, a circuital model able to predict the antenna impedance locus calculated in the full-wave electromagnetic solver is developed with the aim of replacing the full-wave simulations for the probe positioning. This is accomplished by the use of a transmission-line model with a set of parameters derived to fit its impedance locus to the one obtained in the full-wave simulation [4]. Since this transmission line model adapts its input impedance to fit the one from the full-wave simulation, at each algorithm iteration, it is an adaptive model per nature, so it was named ATLM – Adaptive Transmission Line Model. In Section 2, the ATLM is described in detail and some design examples are given to demonstrate its applicability.

Similar to what occurs with conformal microstrip antennas, the literature does not provide a great number of techniques to guide the design of conformal microstrip arrays. Among these design techniques, there are, for example, the Dolph-Chebyshev design and the Genetic Algorithms [9]. However, the results provided by the Dolph-Chebyshev design are not accurate for beam steering [10], once it does not take the radiation patterns of the array elements into account in its calculations, i.e., for this pattern synthesis technique, the array is composed of only isotropic radiators; hence it implies errors in the main beam position and sidelobes levels when the real patterns of the array elements are considered. On the other hand, the Genetic Algorithms can handle well the radiation patterns of the array elements and guarantee that the sidelobes assume a level better than a given specification R [9]. Nonetheless, to control the array directivity [11], it is important that all these sidelobes have the same level R, but to obtain this type of result Genetic Algorithms frequently requires a high number of iterations which increases the design time. Thus, in Section 3, an elegant procedure is employed, based on the solution of linearly constrained least squares problems [12], to the design of conformal microstrip arrays. Not only does this algorithm take the radiation pattern of each array element into account, but it also as-

sures that a determined number of sidelobes levels have the same value, so to get optimized array directivity. And, to obtain more accurate results, the radiation patterns of the array elements, which feed the developed procedure, are evaluated from the array full-wave simulation data. In this work, the CST® Version 2012 was used to get these data. The proposed design technique was coded in the Mathematica® package [13] to create a computer program capable of assisting the design of conformal microstrip arrays. Some examples are given in this section to illustrate the use and effectiveness of this computer program.

Another concern for designing conformal microstrip arrays is how to implement a feed network that can impose appropriate excitations (amplitude and phase) on the array elements to synthesize a desired radiation pattern. Some microstrip arrays used in tracking systems, for example, employ the Butler Matrix [11] as a feed network. Nevertheless, this solution can just accomplish a limited set of look directions and cannot control the sidelobes levels. Hence, in this work, in order not to limit the number of radiation patterns that can be synthesized, an active circuit, composed of phase shifters and variable gain amplifiers, is adopted to feed the array elements. Expressions for calculating the phase shifts and the gains of these components are addressed in Section 4, as well as some design examples are provided to demonstrate their applicability.

2. Algorithm for conformal microstrip antennas design

The main property of the proposed ATLM is to allow the prediction of the impedance locus determined in the antenna full-wave analysis when one of its geometric parameters is modified, for instance, the probe position, thereby replacing full-wave simulations in probe position optimization. It results in a dramatic computational time saving, since a circuital simulation is usually at least 1000 times faster than a full-wave one. In this section, the ATLM is described in detail and some design examples are provided to highlight its advantages.

2.1. Algorithm description

In order to describe the algorithm for the design of conformal microstrip antennas, for the sake of simplicity, let us first consider a probe-fed planar microstrip antenna with a gular patch of length L_{pa} and width W_{pa}, mounted on a dielectric substrate of thickness h_s, relative permittivity ε_r, and loss tangent tanδ, such as the one shown in Figure 1(a). The antenna feed probe is positioned d_p apart from the patch centre. For the following analysis, it is adopted that the antenna resonant frequency f_r is controlled by the length L_{pa} and once the probe is located along the x-axis, it excites the TM_{10} mode, whose main fringing field is also represented in Figure 1(a). Despite this geometry being of planar type, the same model parameters are used to describe the conformal quasi-rectangular microstrip antennas illustrated in Figure 1(b), 1(c) and 1(d), and consequently the algorithm is valid as well.

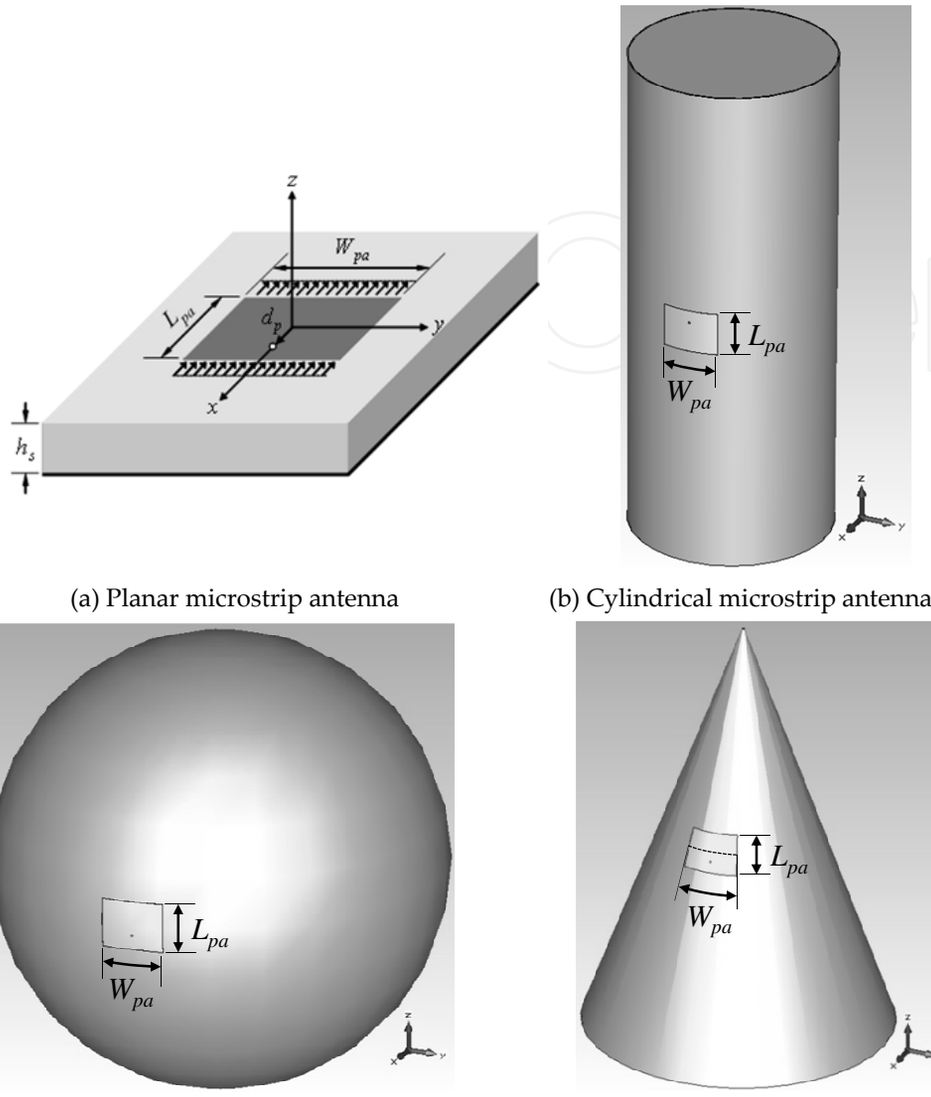

(a) Planar microstrip antenna

(b) Cylindrical microstrip antenna

(c) Spherical microstrip antenna

(d) Conical microstrip antenna

Figure 1. Microstrip antennas studied in this chapter

It is convenient to write both the probe position d_p and patch width W_{pa} as functions of the patch length L_{pa}, to establish a standard set of control variables. Hence, the probe position is written as

$$d_p = R_p L_{pa}, 0 < R_p \leq 0.5, \tag{1}$$

and the patch width as follows

$$W_{pa} = R L_{pa}, R \geq 1. \tag{2}$$

Therefore, the standard set of control variables is composed of L_{pa} ,R(patch width to patch length ratio) and R_p (probe position to patch length ratio). The variables L_{pa} and R_p will be used in the algorithm to control its convergence and the variable R will be defined by specification, based on the desired geometry (rectangular, square). Usually, W_{pa} is made 30% higher than L_{pa} , i.e., R=1.3 [14].

In this work, it is considered that the resonant frequency f_r occurs when the magnitude of the antenna reflection coefficient reaches its minimum value. Under this assumption,

$$\left|\Gamma_a(f_r)\right| = \min_f \left|\Gamma_a(f)\right|, \text{ for } f \in [f_1, f_2], \tag{3}$$

in which $\Gamma_a(f)$ is the reflection coefficient determined in the antenna full-wave analysis, f_1 and f_2 are the minimum and maximum frequencies that define the simulation domain $[f_1, f_2]$. For electrically thin radiators it is usually enough to choose f_1=0.95f_0 and f_2=1.05f_0, where f_0 is the desired operating frequency, and whether the microstrip antenna is electrically thick, then f_1=0.80f_0 and f_2=1.20f_0, in order to locate f_r between f_1 and f_2 in the first algorithm iteration.

Since the antennas design will be conducted in an iterative manner, the optimization process of the model needs to be evaluated against optimization goals in order to set a stop criterion. Therefore, let the frequency error be defined as

$$e = \left|\frac{f_r}{f_0} - 1\right| \tag{4}$$

and its maximum value specified as e_{max}. It leads to the first optimization goal, that is,

$$e \le e_{max}. \tag{5}$$

The second optimization goal is expressed by means of

$$\left|\Gamma_a(f_r)\right| < \Gamma_{min}, \tag{6}$$

where Γ_{min} is a positive real number defined by specification. So, the maximum reflection coefficient magnitude observed at the resonant frequency needs to be lower than Γ_{min}.

Now that the main parameters of the design algorithm have been derived, let us focus on the Adaptive Transmission Line Model, depicted in Figure 2. As can be seen, this circuital model is composed of two microstrip lines, μS_1 and μS_2, whose widths are equal to W_{pa} , an

ideal transmission line TL_p – with characteristic impedance $Z_p$and electrical length $\angle E_l$ (in degrees) given by

$$\angle E_l = 360 h_s \left(\frac{c_0}{f\sqrt{\varepsilon_r}} \right)^{-1}, \tag{7}$$

where c_0 is the speed of the light in free-space –, a capacitor C, and two load terminations L_s. The ideal transmission line together with the capacitor C were included in the model to account for the impedance frequency shift due to the feed probe. In order to fit the input impedance of this model to the one determined in the antenna full-wave analysis, the reflection coefficients at the terminals of the loads L_s are written as

$$\Gamma_f(f) = (a_0 + a_1 f) e^{-j(b_0 + b_1 f)}, \tag{8}$$

in which $\Gamma_f(f)$ is the reflection coefficient of the equivalent slot of impedance Z_f, and a_0, a_1, b_0, b_1 as well as Z_p and C are the set of parameters that determine the frequency response of the circuital model. It is worth mentioning that this ATLM is valid only if its variables L_{pa} and W_{pa} are kept identical to the ones used in the full-wave analysis.

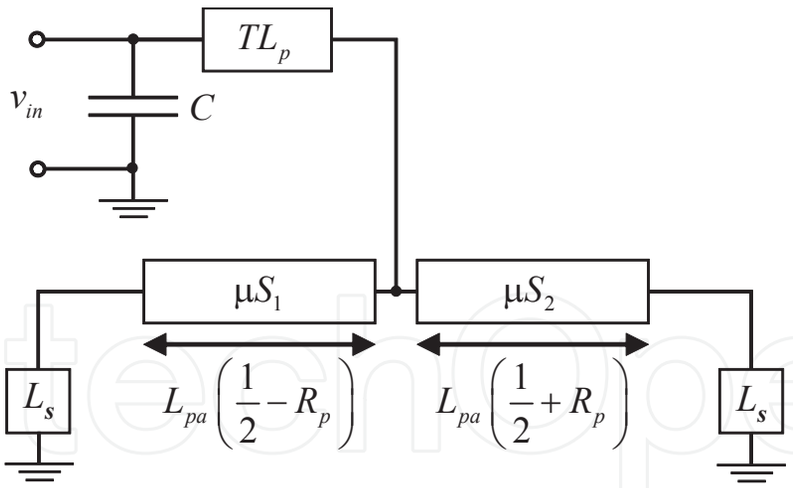

Figure 2. Adaptive transmission line model – ATLM

Once the full-wave simulation $\Gamma_a(f)$ is known, the antenna input impedance $Z_a(f)$ can be easily evaluated. The same is valid for the circuital model analysis in which the reflection coefficient is $\Gamma_c(f)$ and input impedance is $Z_c(f)$. It is important to point out that $\Gamma_a(f)$ data can be exported from the full-wave simulator to the circuit simulator in *Touchstone* format, so $Z_a(f)$ can be utilized by the circuit simulator. The ATLM parameters set is calculated in order to have $\Gamma_c(f)$=$\Gamma_a(f)$ over the simulation domain [f_1,f_2]. The process of finding the values

of this parameters set is called ATLM synthesis and it is done with aid of a Gradient optimization tool, usually available in circuit simulators such as Agilent ADS® [15], as follows.

Consider the generalized load reflection coefficient [16] that is written as

$$\Gamma_L = \frac{Z_L - Z_g^*}{Z_L + Z_g}, \tag{9}$$

in which Z_L is the load impedance and Z_g is the generator impedance, with the superscript * denoting the complex conjugate operator. Since for the ATLM the input voltage v_{in} comes from a generator, it follows that Z_L=Z_c (f). By using a Gradient optimization tool with the goal Γ_L=0 yields

$$Z_c(f) = Z_g^*, \tag{10}$$

after the optimization process.

As we want to ensure that Γ_c (f)=Γ_a (f), i.e., Z_c (f)=Z_a (f), yields

$$Z_g = Z_a^*(f), \tag{11}$$

which is the generator impedance utilized during the ATLM synthesis. On the other hand, for the circuital simulation afterwards, Z_g=Z_0, where Z_0 is the characteristic impedance of the antenna feed network.

Besides, to find a meaningful solution from a physical standpoint, the following two constraints are ensured during the ATLM synthesis

$$\mathrm{Re}\{Z_f\} > 0 \,\text{and}\, \mathrm{Im}\{Z_f\} < 0. \tag{12}$$

The complete probe-fed microstrip antenna design algorithm is depicted through the flowchart in Figure 3, which can be summarized as follows: perform a full-wave antenna simulation for a given patch length and probe position at a certain frequency range (simulation domain), which results in accurate impedance locus data; synthesize the ATLM based on the most updated full-wave simulation data available; optimize the probe position in order to match the antenna to its feed network through circuital simulation and evaluate the resonant frequency; perform patch length scaling; update the full-wave model with the new values of patch length and probe position; and repeat the whole process in an iterative manner until the goals are satisfied.

Generally, it is difficult to get the input impedance of the circuital model perfectly matched to the one obtained from full-wave simulation over the entire simulation domain $[f_1, f_2]$ (i.e., $Z_c(f) \equiv Z_a(f)$), so it is convenient to set the following goal in the Gradient optimizer,

$$|\Gamma_L| \leq \begin{cases} -30\,\text{dB}, f \in \left[(f_0 - \dfrac{f_2 - f_1}{4}), (f_0 + \dfrac{f_2 - f_1}{4}) \right] \\ -20\,\text{dB}, f \notin \left[(f_0 - \dfrac{f_2 - f_1}{4}), (f_0 + \dfrac{f_2 - f_1}{4}) \right] \end{cases}. \tag{13}$$

The previous goal contributes to reduce the number of iterations required by the Gradient optimization tool to determine the set of parameters. It was found that, in general, the required time for the synthesis of the ATLM is at most 5% of the time spent for one full-wave simulation.

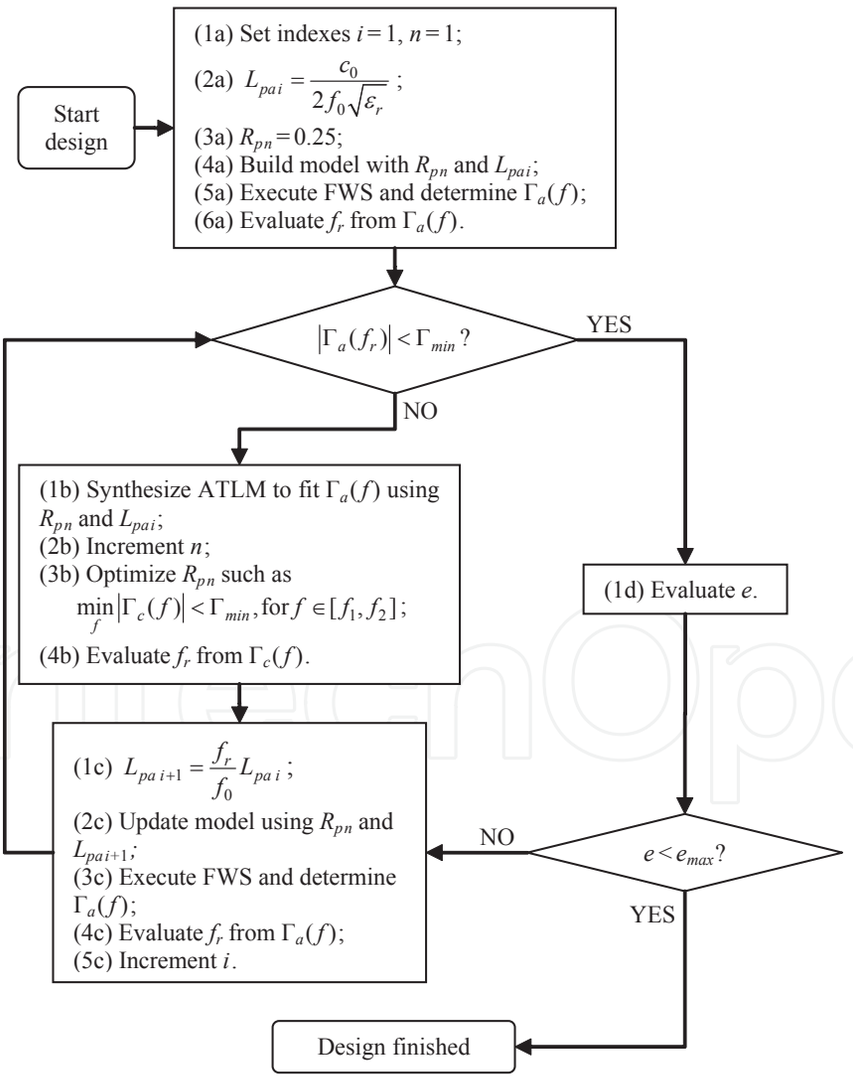

Figure 3. Probe-fed microstrip antenna design algorithm; FWS – Full-Wave Simulation

Regarding the probe position optimization, algorithm step 3b, it can be performed manually by means of a tuning process, a usual feature found in circuit simulators. Thus, R_p is tuned in order to minimize the magnitude of the input reflection coefficient of the circuital model. If desired, the optimization process can be performed employing an optimization tool, e.g., Gradient, Random, also available in circuit simulators. Usually, each circuital analysis takes no longer than 1 second using a simulator such ADS®. But, if one desires to create its own code for the ATLM circuital analysis and probe position optimization, a simple rithm can be implemented to seek the $R_p$that minimizes $|\Gamma_c(f)|$, and the computational time will be greatly reduced as well.

2.2. Applications

To illustrate the use of the technique proposed before, let us first consider the design of a cylindrical microstrip antenna (Figure 1(b)) with a quasi-rectangular metallic patch mounted on a cylindrical dielectric substrate with a thickness h_s=0.762mm, relative permittivity ε_r= 2.5 and loss tangent tan δ = 0.0022, which covers a copper cylinder (ground layer) with a 60.0-mm radius and 300.0-mm height. The patch centre is equidistant from the top and bottom of the copper cylinder. This radiator was designed to operate at f_0 = 3.5 GHz and the algorithm parameters were chosen as e_{max}=0.1×10^{-2}, Γ_{min}=3.16×10^{-2} (return loss of 30dB), and W_{pa}=1.3L_{pa}. Once it is an electrically thin antenna, the simulation domain was given by f_1 =0.95f_0 and f_2 =1.05f_0.

Following the algorithm (Figure 3), a model was built (step 4a) in the CST® software with L_{pa1} =27.11mm and R_{p1} =0.25, and a first full-wave simulation was performed (step 5a). From the analysis of the obtained reflection coefficient $\Gamma_a(f)$, the determined resonant frequency was f_r=3.384GHz (step 6a) and the reflection coefficient magnitude was -17dB, thus higher than the desired maximum of -30 dB (Figure 4(b)).

Hence, at the first decision point of the algorithm, the reflection coefficient magnitude at resonance is not lower than Γ_{min}, so one must go to the step 1b. Then ATLM was synthesized for L_{pa1} =27.11mm and R_{p1} =0.25 and its parameters set was derived with the aid of the Gradient optimization tool of ADS®. After 55 iterations of the Gradient tool, the following parameters set was found: Z_p=94Ω, C=0.87pF, a_0 =-0.58, a_1 =3.83×10^{-10}s, b_0 =-6.54, and b_1 = 2.21×10^{-9} s. The full-wave impedance locus and the one obtained from circuital simulation of the synthesized ATLM are shown in Figure 4(a), and it can be seen that the locus determined though circuital simulation fits very well the full-wave one.

With the circuital model available, the probe position was optimized through manual tuning of the variable R_p, and since for step 3b it is desired that the reflection coefficient magnitude at the resonance be below Γ_{min}, R_p was tuned such as the ATLM impedance locus crossed the Smith Chart centre (Figure 4(a)), leading to R_{p2} =0.21. The resonant frequency obtained from the circuital simulation with this probe position (step 4b) was f_r=3.392GHz. Following the algorithm, the next step was the scaling of patch length (step 1c) leading to L_{pa2} =26.28mm. After updating the full-wave model with these parameters, a full-wave simulation was executed (step 3c) resulting f_r=3.480GHz with a reflection coefficient magnitude of -54dB (Figure 4(b)). Since $|\Gamma_a|<\Gamma_{min}$, the next step was step 1d where it was found that e=0.57×10^{-2},

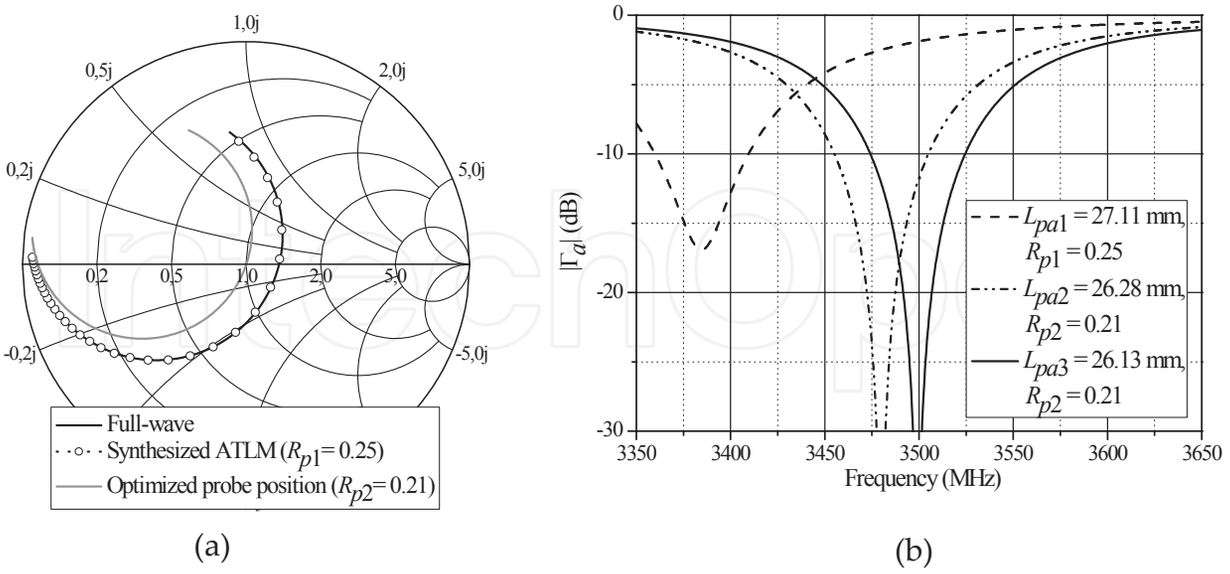

Figure 4. Iterations of the algorithm for the probe-fed cylindrical microstrip antenna design: (a) impedance loci of the full-wave and circuital simulations, (b) reflection coefficient magnitude for the full-wave simulations

higher than e_{max} , thus the algorithm went to step 1c, where a second patch length scaling was done leading to L_{pa3} =26.13mm. A last full-wave simulation with R_{p2} =0.21 and L_{pa3} =26.13mm was performed resulting in e=0.03×10^{-2} and return loss of 54dB at resonance, thus satisfying all specifications. This design required only three full-wave simulations in order to guarantee all specifications, what demonstrates the efficiency of the proposed design technique.

Now let us design a probe-fed spherical microstrip antenna, such as the one illustrated in Figure 1(c). A copper sphere (ground layer) of 120.0-mm radius is covered with a dielectric substrate of constant thickness h_s=0.762mm, relative permittivity ε_r=2.5 and loss tangent tanδ=0.0022. A quasi-rectangular patch with length L_{pa} and width W_{pa} is printed on the surface of the dielectric substrate. The design specifications were the same used previously and the steps of the algorithm followed a path similar to the one in the design of the cylindrical radiator. Once again, the algorithm took only three full-wave simulations to perform the design, as observed in Figure 5(a). The ATLM parameter set found was Z_p=91Ω, C=0.63 pF, a_0 = 6.69×10^{-3}, a_1 = 2.32×10^{-10} s, b_0 = -4.10, b_1 = 1.54×10^{-9} s, and the resulting patch parameters were R_{p2} =0.20 and L_{pa3} =26.06mm, which led to a final frequency error e=0.03×10^{-2} and 35-dB return loss at resonance.

As a last example, let us consider the design of a conical microstrip antenna with a quasi-rectangular metallic patch, as shown in Figure 1(d). It is composed of a conical dielectric substrate of constant thickness h_s=0.762mm that covers a 280.0-mm-high cone made of copper (ground layer) with a 40.0° aperture. The dielectric substrate has the same electromagnetic characteristics as the ones employed in the previous examples and the patch centre is located at the midpoint of its generatrix. This radiator was designed to operate at f_0 = 3.5

http://dx.doi.org/10.5772/53019

GHz and the algorithm parameters were chosen as e_{max}=0.1×10^{-2}, Γ_{min}=3.16×10^{-2} (return loss of 30dB), and W_{pa}=1.3L_{pa}. By applying the developed algorithm, the ATLM parameters set found was Z_p=104Ω, C=0.33pF, a_0=-0.26, a_1=3.01×10^{-10}s, b_0=-4.01, b_1=1.53×10^{-9}s, and the determined patch parameters were R_{p2}=0.23 and L_{pa3}=26.18mm, which yielded a final frequency error e = 0.01×10^{-2} and 34-dB return loss at resonance, once again supporting the proposed design technique. Figure 5(b) presents the reflection coefficient magnitudes of the three full-wave simulations required to accomplish the conical microstrip antenna design.

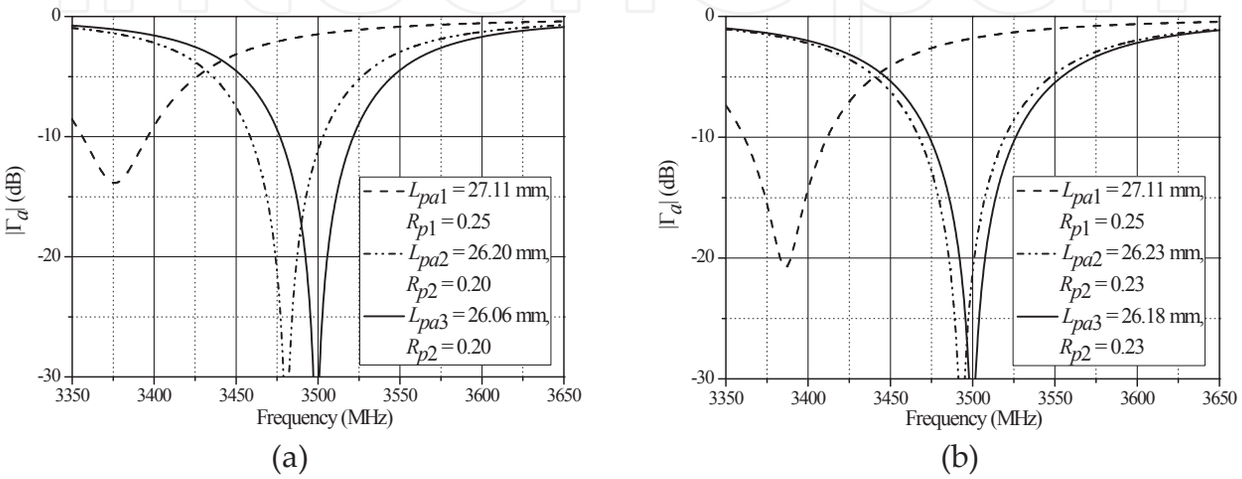

Figure 5. Reflection coefficient magnitudes for each full-wave simulation required for the designs: (a) probe-fed spherical microstrip antenna, (b) probe-fed conical microstrip antenna

3. Radiation pattern synthesis of conformal microstrip arrays

The previous section addressed a computationally efficient algorithm for assisting the design of probe-fed conformal microstrip antennas with quasi-rectangular patches. In order to demonstrate its applicability, three conformal microstrip antennas were synthesized: a cylindrical, a spherical and a conical one. According to what was observed, the algorithm converges very fast, what expedites the antennas' design time.

Another concern in the design of conformal radiators is how to determine the current excitations of a conformal microstrip array to synthesize a desired radiation pattern, in which both the main beam position and the sidelobes levels can be controlled. This section is dedicated to the presentation of a technique employed for the design of conformal microstrip arrays. It is based on the iterative solution of linearly constrained least squares problems [12], so it has closed-form solutions and exhibits fast convergence, and, more important, it takes the radiation pattern of each array element into account in its code, what improves its accuracy. These radiation patterns are determined from the output data obtained through the conformal microstrip array analysis in a full-wave electromagnetic simulator, such as CST® and

HFSS®. Once those data are available, polynomial interpolation is utilized to write simple closed-form expressions that represent adequately the far electric field radiated by each array element, which makes the technique numerically efficient.

The developed design technique was implemented in the Mathematica® platform giving rise to a computer program – called CMAD (Conformal Microstrip Array Design) – capable of performing the design of conformal microstrip arrays. The Mathematica® package, an integrated scientific computer software, was chosen mainly due to its vast collection of built-in functions that permit implementing the respective algorithm in a short number of lines, in addition to its many graphical resources. At the end of the section, to illustrate the CMAD ability to synthesize the radiation pattern of conformal microstrip arrays, the synthesis of the radiation pattern of three conformal microstrip array topologies is considered. First, a microstrip antenna array conformed onto a cylindrical surface is analysed. Afterwards, a spherical microstrip array is studied. Finally, the synthesis of the radiation pattern of a conical microstrip array is presented.

3.1. Algorithm description

The far electric field radiated by a conformal microstrip array composed of N elements and embedded in free space, assuming time-harmonic variations of the form $e^{j\omega t}$, can be written as

$$E = \mathbb{C}\frac{e^{-jk_0 r}}{r} I^t \cdot v(\theta, \phi), \tag{14}$$

where the constant $\mathbb{C}$ is dependent on both the free-space electromagnetic characteristics, μ_0 and ε_0, and the angular frequency ω, $k_0=\omega\{\mu_0 \varepsilon_0\}^{1/2}$ is the free-space propagation constant,

$$I^t = \begin{bmatrix} I_1 & \cdots & I_N \end{bmatrix}, \tag{15}$$

with I_n, $1 \le n \le N$, representing the current excitation of the n-th array element and the superscript t indicates the transpose operator,

$$\boldsymbol{v}(\theta,\phi) = \begin{bmatrix} \boldsymbol{g}_1(\theta,\phi) \\ \vdots \\ \boldsymbol{g}_N(\theta,\phi) \end{bmatrix}, \tag{16}$$

in which $\boldsymbol{g}_n(\theta,\phi)$, $1 \le n \le N$, denotes the complex pattern of the n-th array element evaluated in the global coordinate system. Boldface letters represent vectors throughout this chapter.

Based on (14), the radiation pattern of a conformal microstrip array can be promptly calculated using the relation

$$|I^t \cdot \boldsymbol{v}(\theta,\phi)|^2 = w^\dagger \cdot [\boldsymbol{v}(\theta,\phi) \cdot \boldsymbol{v}^\dagger(\theta,\phi)] \cdot w, \quad (17)$$

where the complex weight w is equal to I^*, the superscript * represents the complex conjugate operator and † indicates the Hermitian transpose (complex conjugate transpose operator). Therefore, the radiation pattern evaluation requires the knowledge of both complex weight w and vector$\boldsymbol{v}(\theta,\phi)$.

Once the array elements are chosen and their positions are predefined, to determine the vector v (θ, ϕ) tor $\boldsymbol{v}(\theta,\phi)$ it is necessary to calculate the complex patterns $\boldsymbol{g}_n(\theta,\phi)$, $1 \le n \le N$, of the array elements. For conformal microstrip arrays there are some well-known techniques to accomplish this [1], for example, the commonly used electric surface current method [17-19]. However, when this technique is employed to analyse cylindrical or conical microstrip arrays, for instance, it cannot deal with the truncation of the ground layer and the diffraction at the edges of the conducting surfaces that affect the radiation pattern. Moreover, the expressions derived from this method for calculating the radiated far electric field frequently involve Bessel and Legendre functions. Nevertheless, as extensively reported in the literature [20], the evaluation of these functions is not fast and requires good numerical routines. Hence, to overcome these drawbacks and to get more accurate results, in this chapter, the complex patterns $\boldsymbol{g}_n(\theta,\phi)$ are determined from the data obtained through the conformal microstrip array analysis in the CST® package. It is important to point out that other commercial 3D electromagnetic simulators, such as HFSS®, can also be used to assist the evaluation of the complex patterns $\boldsymbol{g}_n(\theta,\phi)$, since they are able to take into account truncation of the ground layer and diffraction at the edges of the conducting surfaces.

From the array full-wave simulation data, polynomial interpolation is applied to generate simple closed-form expressions that represent adequately the far electric field (amplitude and phase) radiated by each array element. In this work, the degree of the interpolation polynomials is established from the analysis of the *RMSE* (root-mean-square error), which provides a measure of similarity between the interpolated data and the ones given by CST®. For the following examples the interpolation polynomials' degrees are defined aiming at a *RMSE* less than 0.02.

Considering the previous scenario, to synthesize a radiation pattern in a given plane, it just requires the determination of the current excitations I_n present in the complex weight w. Figure 6 illustrates a typical specification of a radiation pattern containing information about the main beam direction α, the intervals intervals $[\theta_a, \theta_b]$ and $[\theta_c, \theta_d]$ where the sidelobes are located as well as the maximum level R that can be assumed for them.

Based on (17) and following [12], a constrained least squares problem is established in order to locate the main beam at the α direction,

$$\min_w w^\dagger \cdot A \cdot w \quad (18)$$

subject to the constraints

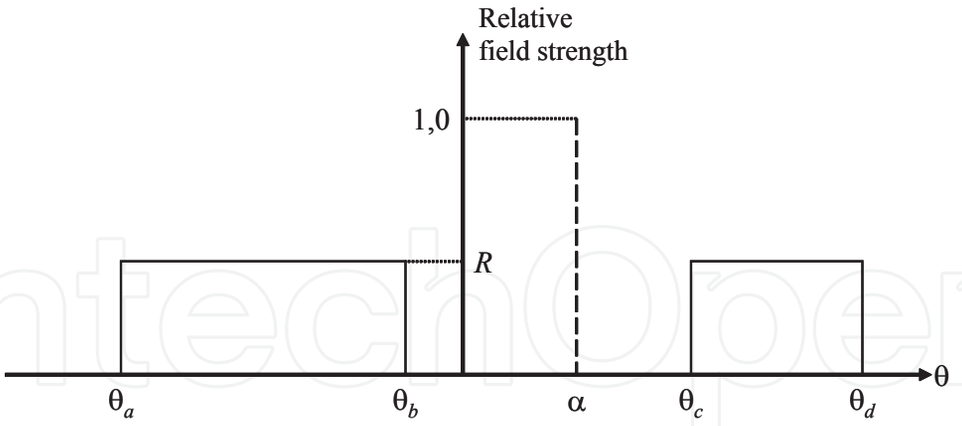

Figure 6. Typical specification of a radiation pattern in a given plane

$$\boldsymbol{v}_s^{\dagger} \cdot w = 1, \tag{19}$$

$$\mathrm{Re}\{\boldsymbol{v}_d^{\dagger} \cdot w\} = 0, \tag{20}$$

in which $\boldsymbol{v}_s = \boldsymbol{v}(\alpha,\phi')$, $\boldsymbol{v}_d = \partial \boldsymbol{v}(\theta,\phi)/\partial\theta\,|_{(\theta\,,\,\phi)\,=\,(\alpha\,,\,\phi')}$, ϕ' is the ϕ coordinate of the plane where the pattern is being synthesized, and

$$A = \frac{1}{2}\sum_{\ell=1}^{L} \boldsymbol{v}(\theta_\ell,\phi') \cdot \boldsymbol{v}^{\dagger}(\theta_\ell,\phi'), \tag{21}$$

with the angles θ_ℓ, ℓ=1,2,…,L, uniformly sampled in the sidelobes intervals $[\theta_a,\theta_b]$ and $[\theta_c,\theta_d]$. In the next examples the adopted step size between consecutive θ_ℓ is equal to 0.1° (for each of the sidelobes intervals).

In order to find a closed-form solution to the problem defined by (18) to (20), we determine its real counterpart [21], that is,

$$\min_{\tilde{w}} \tilde{w}^{t} \cdot \tilde{A} \cdot \tilde{w} \tag{22}$$

subject to the following linear constraints

$$\tilde{C}^{t} \cdot \tilde{w} = \tilde{f}, \tag{23}$$

where

$$\tilde{w} = \left[\mathrm{Re}\{w\} \quad \mathrm{Im}\{w\} \right]^t, \tag{24}$$

$$\tilde{A} = \begin{bmatrix} \mathrm{Re}\{A\} & -\mathrm{Im}\{A\} \\ \mathrm{Im}\{A\} & \mathrm{Re}\{A\} \end{bmatrix}, \tag{25}$$

$$\tilde{C} = \left[\tilde{\boldsymbol{v}}_s \quad \hat{\boldsymbol{v}}_s \quad \tilde{\boldsymbol{v}}_d \right], \tag{26}$$

$$\tilde{f} = \left[1 \quad 0 \quad 0 \right]^t, \tag{27}$$

with

$$\tilde{\boldsymbol{v}}_s = \left[\mathrm{Re}\{\boldsymbol{v}_s\} \quad \mathrm{Im}\{\boldsymbol{v}_s\} \right]^t, \tag{28}$$

$$\hat{\boldsymbol{v}}_s = \left[-\mathrm{Im}\{\boldsymbol{v}_s\} \quad \mathrm{Re}\{\boldsymbol{v}_s\} \right]^t, \tag{29}$$

$$\tilde{\boldsymbol{v}}_d = \left[\mathrm{Re}\{\boldsymbol{v}_d\} \quad \mathrm{Im}\{\boldsymbol{v}_d\} \right]^t. \tag{30}$$

The closed-form solution to the problem (22) and (23) is

$$\tilde{w} = \tilde{A}^{-1} \cdot \tilde{C} \cdot \left(\tilde{C}^t \cdot \tilde{A}^{-1} \cdot \tilde{C} \right)^{-1} \cdot \tilde{f}, \tag{31}$$

from which the complex weight w is promptly evaluated.

After solving the problem (18)-(20) the main beam is located at the α-direction. Nevertheless, it cannot be assured that the sidelobes levels are below the threshold R. In order to get it, the complex weight w is updated by residual complex weights Δw, as follows:

$$w \leftarrow w + \Delta w. \tag{32}$$

A constrained least squares problem, similar to (18)-(20), that ensures the sidelobes levels, is set up for the purpose of calculating the residual complex weights Δw, that is,

$$\min_{\Delta w} \Delta w^{\dagger} \cdot A \cdot \Delta w \tag{33}$$

subject to the constraints

$$\boldsymbol{v}_s^{\dagger} \cdot \Delta w = 0\,, \tag{34}$$

$$\mathrm{Re}\{\boldsymbol{v}_d^{\dagger} \cdot \Delta w\} = 0\,, \tag{35}$$

$$\boldsymbol{v}_i^{\dagger} \cdot \Delta w = f_i\,,\ i = 1,2,\ldots,m\,, \tag{36}$$

in which $\boldsymbol{v}_i=\boldsymbol{v}(\theta_i,\phi')$, with θ_i denoting the θ coordinate of the i-th sidelobe, m is the number of sidelobes whose levels are being modified (the maximum m is equal to N–2), and the complex function f_i can be evaluated through

$$f_i = (R - |\,c_i\,|)\frac{c_i}{|\,c_i\,|}\,, \tag{37}$$

where

$$c_i = w^{\dagger} \cdot \boldsymbol{v}_i\,. \tag{38}$$

It is important to point out that the constraints (34) and (35) retain the main beam located at the α-direction, and the ones in (36) are responsible for conducting the sidelobes levels to the threshold R. A closed-form solution to the problem (33)-(36) is also determined from its real counterpart, analogous to the solution to the problem (18)-(20). The problem (33)-(36) is iteratively solved until the sidelobes levels reach the desired value R. Notice that at each iteration the maximum number of sidelobes whose levels are controlled is equal to N – 2, i.e., if the array radiation pattern has more than N – 2 sidelobes, we choose the N – 2 sidelobes with the highest levels to apply the constraints (36).

The radiation pattern synthesis technique described before was implemented in the Mathematica® platform with the aim of developing a CAD – called CMAD – capable of performing the design of conformal microstrip arrays. The inputs required to start the design procedure in the CMAD program are the Text Files (.txt extension) containing the points that describe the complex patterns of each array element – obtained from the conformal microstrip array simulation in CST® package –, the look direction α, the maximum sidelobes level R, and the starting and ending points of the intervals $[\theta_a,\theta_b]$ and $[\theta_c,\theta_d]$ where they are located. As a result, the CMAD returns the current excitations and the synthesized pattern. It is worth mentioning that the use of interpolation polynomials to describe the complex patterns expedites the evaluation of both vector $\boldsymbol{v}(\theta,\phi)$ and its derivative; consequently, the CMAD's run

http://dx.doi.org/10.5772/53019

time is diminished. In the following three sections, examples of radiation pattern synthesis are provided to demonstrate the capability of the developed CMAD program.

3.2. Cylindrical microstrip array

To illustrate the described pattern synthesis technique, let us first consider the design of a five-element cylindrical microstrip array, such as the one shown in Figure 7(a). For this array, the cylindrical ground layer is made out of copper cylinder with a 60.0-mm radius and a 300.0-mm height. The employed dielectric substrate has a relative permittivity ε_r = 2.5, a loss tangent tan δ = 0.0022 and its thickness is h_s = 0.762 mm. The array patches are identical to the one designed in Section 2.2 to operate at 3.5 GHz. The five elements are fed by 50-ohm coaxial probes positioned 5.49 mm apart from the patches' centres and the interelement spacing was chosen to be λ_0 / 2 = 42.857 mm (λ_0 is the free-space wavelength at 3.5 GHz).

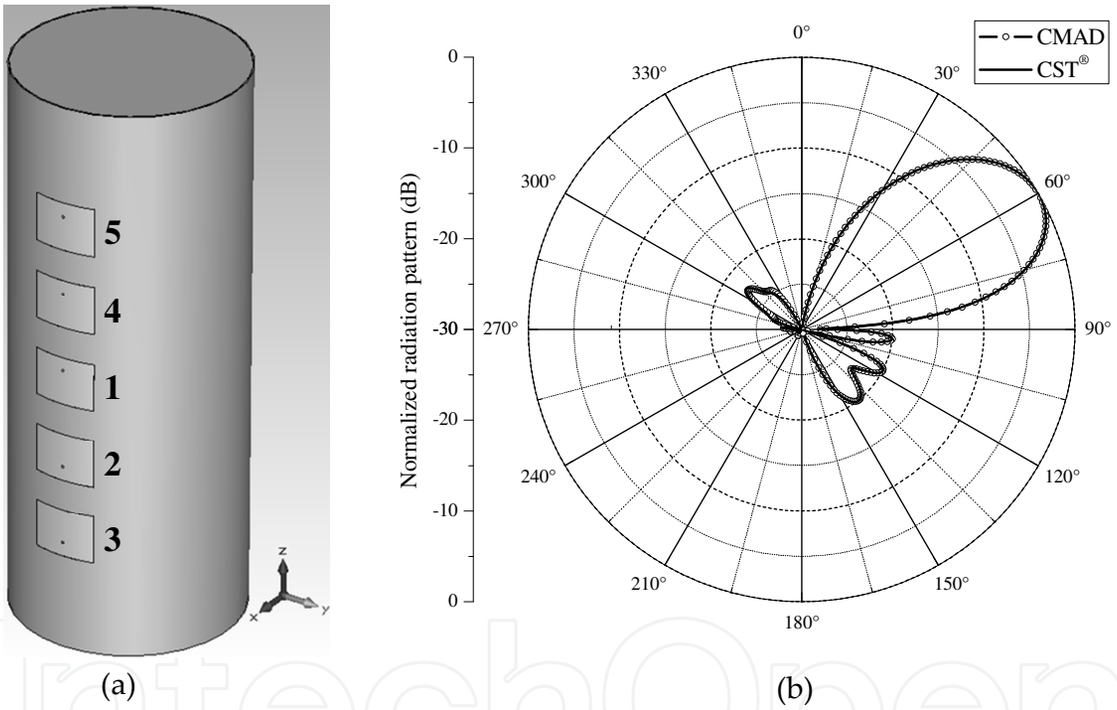

Figure 7. (a)Five-element cylindrical microstrip array, (b) E_θ radiation pattern: *xz*-plane, $\alpha = 60°$, R = -20 dB, and f = 3.5 GHz

It is important to point out that the elements close to the ends of the ground cylinder have significantly different radiation patterns than those close to the centre of this cylinder; however, the technique developed in this chapter can handle well this aspect, different from the common practice that assumes the elements' radiation patterns are identical [22]. To clarify this difference among the patterns, Figure 8 shows the radiation patterns of the elements number 1 and 5. In Figure 8(a) they were evaluated in CST® and in Figure 8(b) they were determined from the interpolation polynomials. As observed, there is an excellent agreement between the radiation patterns described by the interpolation polynomials and the ones provided by CST®, even in the back region, where the radiation pattern exhibits low

level and oscillatory behaviour. It validates the use of polynomial interpolation functions to represent the far electric field radiated by the conformal array elements.

For this cylindrical array, let us consider that the radiation pattern in the *xz*-plane must have the main beam located at $\alpha = 60°$ and the maximum sidelobe level allowed is $R = -20$ dB. By using the CMAD program, we get both the array normalized current excitations, depicted in Table 1, and the synthesized radiation pattern, shown in Figure 7(b). In order to validate these results, we provide the normalized current excitations (Table 1) for the array simulation in CST®. The radiation pattern evaluated in CST® is also represented in Figure 7(b). According to what is observed, there is an excellent agreement between the radiation pattern given by the CMAD and the one calculated in CST®, thus validating the developed technique to design cylindrical microstrip arrays.

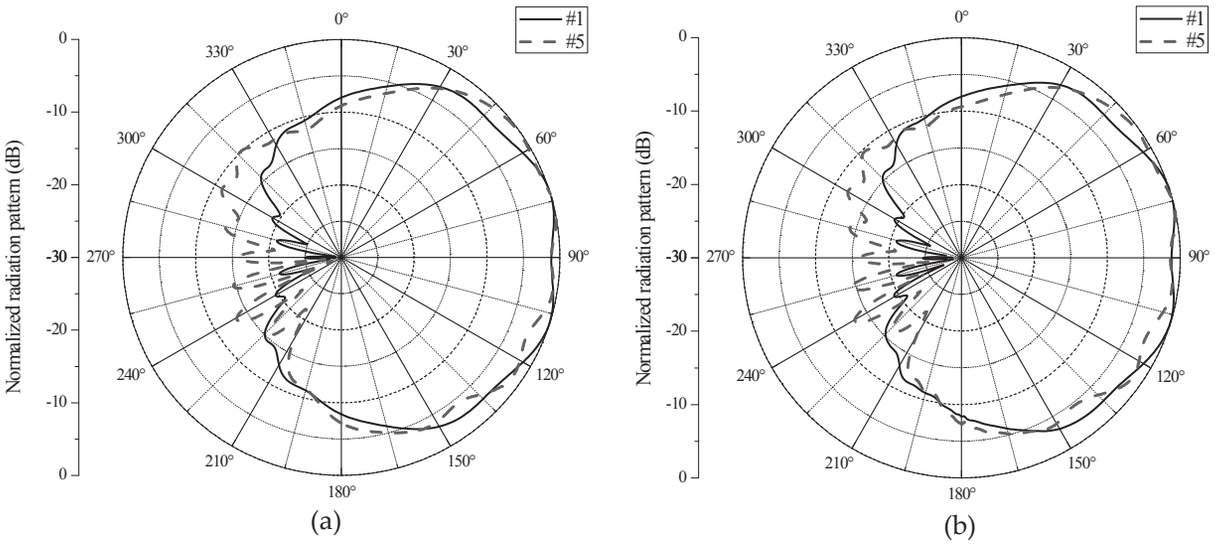

Figure 8. E_θ radiation patterns – elements number 1 and 5: *xz*-plane and $f = 3.5$ GHz. (a) CST® and (b) interpolation polynomials

Element Number	Normalized Current Excitation
1	1.0∠0.0°
2	0.800∠-82.394°
3	0.360∠6.211°
4	0.781∠-90.315°
5	0.617∠172.593°

Table 1. Cylindrical microstrip array: normalized current excitations

http://dx.doi.org/10.5772/53019

3.3. Spherical microstrip array

Another conformal microstrip array topology used to demonstrate the CMAD's ability to synthesize radiation patterns is the five-element spherical microstrip array, which operates at 3.5 GHz, illustrated in Figure 9(a). For this array, the selected ground layer is a copper sphere with a radius of 120.0 mm. A typical microwave substrate (ε_r = 2.5, tan δ = 0.0022 and h_s = 0.762 mm) covers all the ground sphere and the array patches are the same as the ones designed in Section 2.2. The angular interelement spacing in the θ-direction was chosen to be 20.334°, which corresponds to an arc length of λ_0 / 2 onto the external microwave substrate surface.

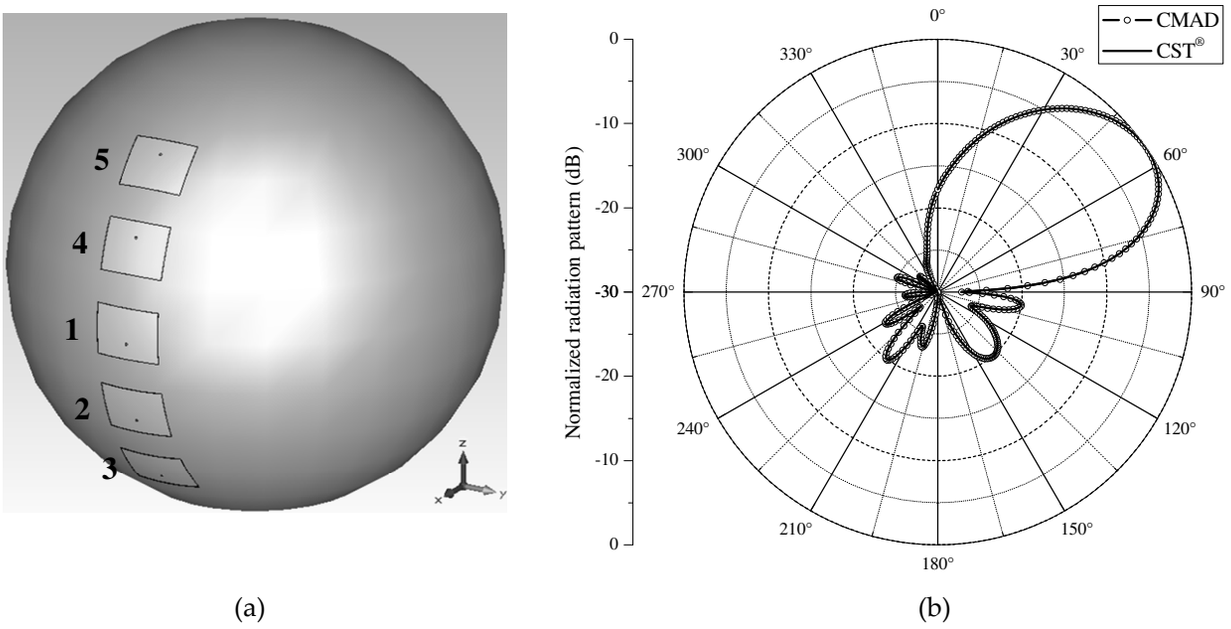

(a) (b)

Figure 9. (a) Five-element spherical microstrip array, (b) E_θ radiation pattern: *xz*-plane, α = 55°, *R* = -20 dB, and *f* = 3.5 GHz

In this case, the synthesized radiation pattern in the *xz*-plane must have its main beam located at α = 55.0° direction and the maximum sidelobe level cannot exceed -20 dB. After entering these requirements in the CMAD program, it outputs the normalized current excitations (Table 2) and the synthesized radiation pattern (Figure 9(b)). To verify these results, the normalized current excitations were loaded into the spherical microstrip array simulation conducted in the CST® software. The radiation pattern obtained is also shown in Figure 9(b) for comparisons purposes. As seen, the radiation pattern given by the CMAD program and the one determined in CST® show a very good agreement, thus supporting the proposed radiation pattern synthesis technique. It is important to point out that the interelement spacing could be varied if the array directivity needs to be altered.

Element Number	Normalized Current Excitation
1	0.680∠264.460°
2	0.252∠-6.059°
3	0.160∠156.639°
4	1.0∠0.0°
5	0.728∠-36.758°

Table 2. Spherical microstrip array: normalized current excitations

3.4. Conical microstrip array

Finally, let us consider the radiation pattern synthesis of the four-element conical microstrip array presented in Figure 10(a). For this array, the ground layer is a 280.0-mm-high cone made of copper with a 40.0° aperture. This cone is covered with a dielectric substrate of constant thickness h_s = 0.762 mm, relative permittivity ε_r = 2.5 and loss tangent tan δ = 0.0022. The array elements are identical to the one designed in Section 2.2, so they have a length of 26.18 mm in the generatrix direction, an average width of 34.03 mm in the ϕ-direction, and the 50-ohm coaxial probes are located 6.02 mm apart from the patches' centres toward the ground cone basis. The interelement spacing in the generatrix direction is of 42.857 mm (= λ_0 / 2) as well as the centre of the element #1 is 110.0 mm apart from the cone apex in this same direction.

The radiation pattern specifications for this synthesis are: main beam direction α = 70° and maximum sidelobe level R = -20 dB, both in the xz-plane. By using the CMAD program, we derive the normalized current excitations, shown in Table 3, and the synthesized radiation pattern in the frequency 3.5 GHz, illustrated in Figure 10(b). Also in Figure 10(b) the array radiation pattern calculated in CST®, considering the normalized current excitations of Table 3, is presented. As observed, the radiation pattern obtained with CMAD matches the one determined in CST®, once again supporting the proposed design approach.

4. Active feed circuit design

As can be seen, the radiation pattern synthesis technique presented in the previous section is suitable for applications that require electronic radiation pattern control, for example. However, it only provides the array current excitations, i.e., to complete the array design it is still necessary to synthesize its feed network. A simple active circuit topology dedicated to feed those arrays can be composed of branches having a variable gain amplifier cascaded to a phase shifter, both controlled by a microcontroller, and a 1 : N power divider, as depicted in

http://dx.doi.org/10.5772/53019

Figure 11. The phase shifters play a role in controlling the phases of the current excitations, as well as the variable gain amplifiers that are responsible for settling their amplitudes. In this section, expressions for calculating the phase shifts ϕ_n and the gains G_n, in terms of the array current excitations and their electrical characteristics, including the self and mutual impedances, are derived. It is worth mentioning that the evaluated expressions take into account the mismatches between the array elements' driving impedances and the characteristic impedance Z_0 of the lines, what improves their accuracy.

At the end of this section, to illustrate the synthesis of the proposed active feed network (Figure 11), the design of the active beamformers of the three conformal microstrip arrays (cylindrical, spherical and conical) that appear along the chapter is described. Furthermore, to validate the phase shifts and gains calculated, the designed feed networks are analysed in the ADS® package.

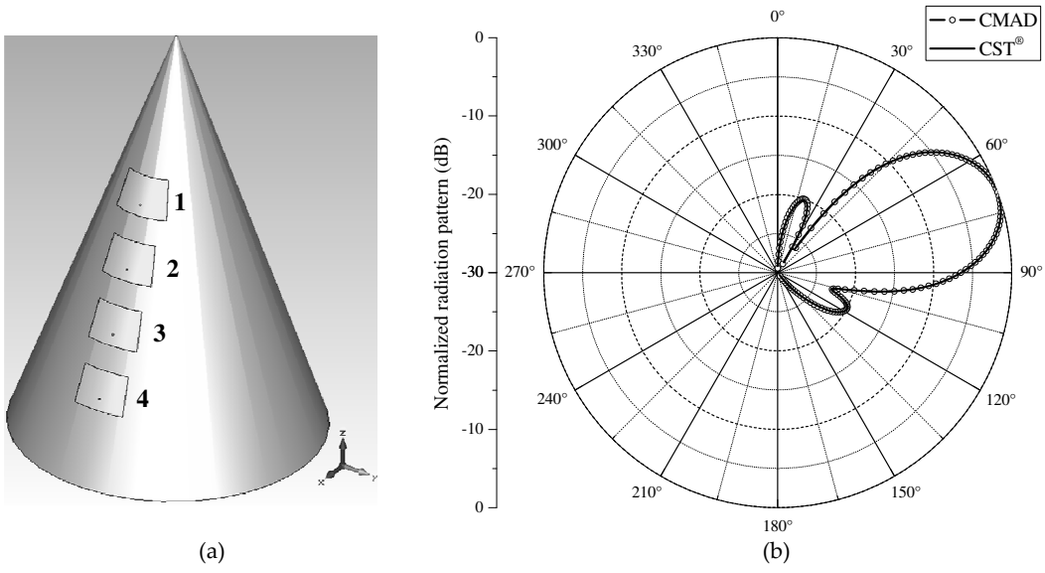

Figure 10. (a) Four-element conical microstrip array, (b) E_θ radiation pattern: *xz*-plane, $\alpha = 70°$, $R = -20$ dB, and $f = 3.5$ GHz

Element Number	Normalized Current Excitation
1	0.574∠-7.835°
2	0.875∠0.149°
3	1.0∠0,0°
4	0.625∠-6.561°

Table 3. Conical microstrip array: normalized current excitations

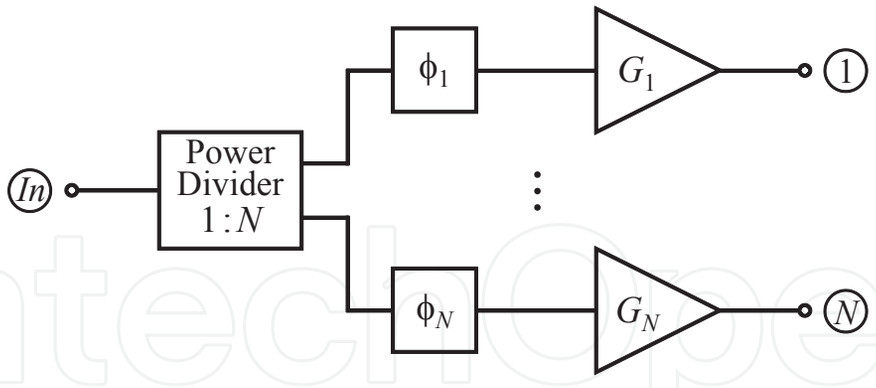

Figure 11. Active feed network

4.1. Design equations

For the analysis conducted here the phase shifters are considered perfectly matched to the input and output lines and produce zero attenuation. Based on these assumptions the scattering matrix $(S_{pf})_n$ of the n-th phase shifter, $1 \le n \le N$, assumes the form

$$(S_{pf})_n = \begin{pmatrix} 0 & e^{j\phi_n} \\ e^{j\phi_n} & 0 \end{pmatrix}, \tag{39}$$

with ϕ_n ($0 \le \phi_n < 2\pi$) representing the phase shift produced by the n-th phase shifter. Notice that the matching requirement can be met to within a reasonable degree of approximation for commercial IC (Integrated Circuit) phase shifters, however those devices frequently exhibit moderate insertion loss. So, to take the insertion loss into account in our analysis model, the gains G_n are either decreased or increased (to compensate the insertion losses).

The variable gain amplifiers are also considered perfectly matched to the input and output lines and they are unilateral devices, i.e., $s_{12n}=0$. Hence, the scattering matrix $(S_a)_n$ of the n-th variable gain amplifier is given by

$$(S_a)_n = \begin{pmatrix} 0 & 0 \\ s_{21n} & 0 \end{pmatrix}, \tag{40}$$

in which s_{21n} denotes the gain (linear magnitude) of the n-th variable gain amplifier. It is worth mentioning that lots of commercial IC variable gain amplifiers have input and output return loss better than 10 dB and exhibit high directivity, therefore, the preceding assumptions are reasonable. More precise results using the scattering parameters of commercial variable gain amplifiers and phase shifters are presented in [23].

http://dx.doi.org/10.5772/53019

Let us examine the operation of the n-th circuit branch. The input power P_n at the terminals of the n-th array element can be calculated by

$$P_n = \frac{1}{2}\mathrm{Re}\{Zin_n\}\,|\,I_n\,|^2, \tag{41}$$

where Zin_n is the driving impedance at the terminals of the n-th array element and can be evaluated using

$$Zin_n = \sum_{\kappa=1}^{N} Z_{n\kappa}\frac{I_\kappa}{I_n} \tag{42}$$

in which $Z_{n\kappa}$ is the n-th array element self-impedance, if n=κ, and the mutual impedance between the n-th and κ-th array elements, if $n \neq \kappa$. In this chapter the self and mutual impedances will be determined from the array simulation data. However, those impedances could also be obtained from the measurements conducted in the array prototype, what certainly would lead to a more accurate feed network design.

Alternatively, the input power at the terminals of the n-th array element can be expressed in terms of the incident power P_{0n} and the reflection coefficient Γin_n at the terminals as

$$P_n = P_{0n}(1-|\,\Gamma in_n\,|^2), \tag{43}$$

with

$$\Gamma in_n = \frac{Zin_n - Z_0}{Zin_n + Z_0}. \tag{44}$$

Combining (41) and (43) results in an expression to evaluate the incident power at the terminals of the n-th array element

$$P_{0n} = \frac{\mathrm{Re}\{Zin_n\}\,|\,I_n\,|^2}{2(1-|\,\Gamma in_n\,|^2)}, \tag{45}$$

which is equal to the n-th variable gain output power, disregarding the losses in the lines.

Based on (45), an equation to determine the gain of the n-th variable gain amplifier is derived:

$$G_n = \frac{P_{0n}}{P_{0m}} = \frac{\mathrm{Re}\{Zin_n\}}{\mathrm{Re}\{Zin_m\}} \frac{1-|\Gamma in_m|^2}{1-|\Gamma in_n|^2} \frac{|I_n|^2}{|I_m|^2}. \tag{46}$$

Notice that to evaluate (46) it is necessary to choose one of the circuit branches as a reference, i.e., the gain of the m-th variable gain amplifier is set equal to 1.0.

It is important to highlight that this formulation has relevant importance for arrays whose mutual coupling among elements is strong [23], since it takes this effect into account. For arrays whose mutual coupling among elements is weak and the array elements self-impedances are close to Z_0, (46) is approximated by

$$G_n \cong \frac{|I_n|^2}{|I_m|^2}. \tag{47}$$

Now, to determine the phase shifts ϕ_n, let us consider the current I_n at the terminals of the n-th array element, that is,

$$I_n = I_{0n} e^{j\phi_n} (1 - \Gamma in_n), \tag{48}$$

in which $I_{0n} e^{j\phi_n}$ is the incident current wave at the terminals of the n-th array element.

Once the currents I_n are provided by the algorithm described in the last section, to calculate ϕ_n the phases of the left and right sides of (48) are enforced to be equal. Then,

$$\phi_n = \delta_{nm} - \arg\{1 - \Gamma in_n\} + \arg\{1 - \Gamma in_m\}, \tag{49}$$

with

$$\delta_{nm} = \arg\{I_n\} - \arg\{I_m\}. \tag{50}$$

Also for the determination of the phase shift ϕ_n, the m-th circuit branch was taken as a reference, i.e., its phase shifter does not introduce any phase shift (ϕ_m=0°) in the signal.

For arrays whose mutual coupling among elements is weak and the array elements self-impedances are close to Z_0, the phase shift ϕ_n (49) reduces to

$$\phi_n \cong \delta_{nm}. \tag{51}$$

http://dx.doi.org/10.5772/53019

The expressions for evaluating the gains G_n (46) and phase shifts ϕ_n (49) were incorporated into the developed computer program CMAD to generate a new module devoted to design active feed networks, such as the one illustrated in Figure 11. The inputs required to start the circuit design are the array current excitations and the *Touchstone* File (.sNp extension) containing the array scattering parameters – obtained from the conformal microstrip array simulation in a full-wave electromagnetic simulator, for example. In the next section, to demonstrate the capability of this new CMAD feature, the feed networks of the three conformal microstrip arrays previously synthesized will be designed.

4.2. Examples

The normalized current excitations found in Tables 1 to 3 and the scattering parameters of the three conformal microstrip arrays synthesized in this chapter (evaluated in CST®) were provided to the CMAD. As results, it returned the gains and phase shifts of the active feed networks that implement the radiation patterns shown in Figures 7(b), 9(b) and 10(b). These values are listed in Table 4.

To verify the validity of the results found in Table 4, the designed active feed networks were analysed in the ADS® package. As an example, Figure 12 shows the simulated feed network for the conical microstrip array. In this circuit, the array is represented through a 4-port microwave network, whose scattering parameters are the same as the ones used by the CMAD, it is fed by a 30-dBm power source with a 50-ohm impedance, and there are four current probes to measure the currents at the terminals of the 4-port microwave network, which correspond to the array current excitations. Table 5 summarizes the current probes readings for the three analysed feed networks. The comparison between the currents given in Table 5 and the ones presented in Tables 1 to 3 shows that these currents are in agreement, thereby validating the design equations derived before.

Branch Number	Cylindrical Array		Spherical Array		Conical Array	
	Gain (dB)	Phase Shift (deg)	Gain (dB)	Phase Shift (deg)	Gain (dB)	Phase Shift (deg)
1	7.4	351.1	11.1	114.6	0.0	0.0
2	5.7	267.6	3.8	205.0	4.2	7.0
3	0.0	0.0	0.0	0.0	5.4	4.1
4	4.9	260.6	14.0	210.3	1.5	356.6
5	2.4	164.0	10.9	173.0	–	–

Table 4. Gains and phase shifts of the designed active feed networks

Branch Number	Cylindrical Array	Spherical Array	Conical Array
1	0.160∠-10.37°	0.249∠113.2°	0.106∠-9.417°
2	0.128∠-92.76°	0.092∠-157.3°	0.161∠-1.432°
3	0.058∠-4.156°	0.059∠5.375°	0.184∠-1.581°
4	0.125∠-100.7°	0.366∠-151.3°	0.115∠-8.141°
5	0.099∠162.2°	0.267∠172.0°	–

Table 5. Current probes readings (in ampere)

5. Conclusion

In summary, a computationally efficient algorithm capable of assisting the design of probe-fed conformal microstrip antennas with quasi-rectangular patches was discussed. Some examples were provided to illustrate its use and advantages. As seen, it can result in significant reductions in design time, since the required number of full-wave electromagnetic simulations, which are computationally intensive – especially for conformal radiators –, is diminished. For instance, the proposed designs could be performed with only three full-wave simulations. Also in this chapter, an accurate design technique to synthesize radiation patterns of conformal microstrip arrays was introduced. The adopted technique takes the radiation pattern of each array element into account in its code through the use of interpolation polynomials, different from the common practice that assumes the elements' radiation patterns are identical. Hence, the developed technique can provide more accurate results. Besides, it is able to control the sidelobes levels, so that optimized array directivity can be achieved. This design technique was coded in the Mathematica® platform giving rise to a computer program, called CMAD, that evaluates the array current excitations responsible for synthesizing a given radiation pattern. To show the potential of the CMAD program, the design of cylindrical, spherical and conical microstrip arrays were exemplified. Finally, an active feed network suitable for applications that require electronic radiation pattern control, like tracking systems, was addressed. The expressions derived for the synthesis of this circuit take into account the mutual coupling among the array elements; therefore they are also suited for array configurations in which the mutual coupling among the elements is strong. These design equations were incorporated into the CMAD code adding to it one more project tool. In order to validate this new CMAD feature, the feed networks of the three conformal microstrip arrays described along the chapter were designed. The obtained results were validated through the feed networks' simulations in the ADS® software.

http://dx.doi.org/10.5772/53019

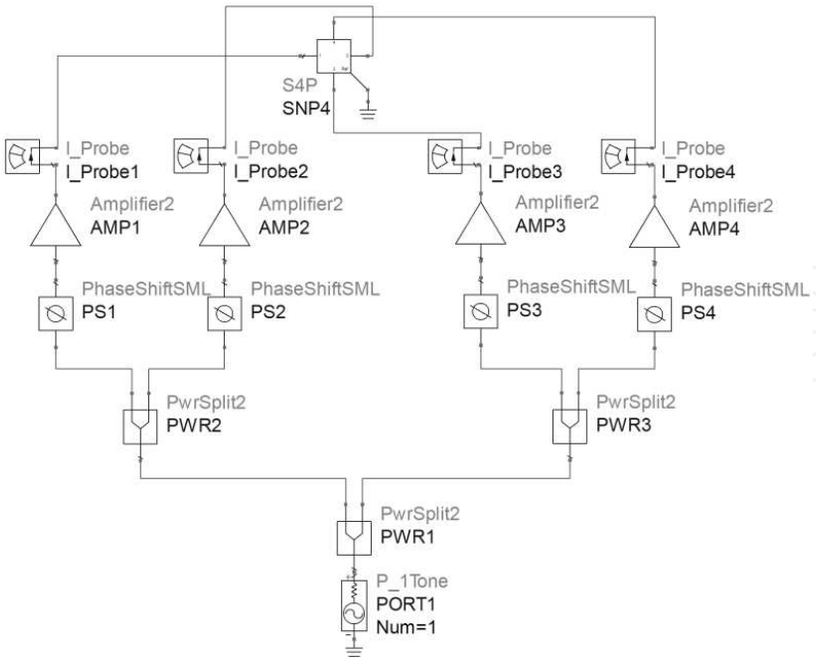

Figure 12. Simulated feed network for the conical microstrip array

Acknowledgements

The authors would like to acknowledge the support given to this work, developed under the project "Adaptive Antennas and RF Modules for Wireless Broadband Networks Applied to Public Safety", with the support of the Ministry of Communications' FUNTTEL (Brazilian Fund for the Technological Development of Telecommunications), under Grant No. 01.09.0634.00 with the Financier of Studies and Projects - FINEP / MCTI.

Author details

Daniel B. Ferreira[1], Cristiano B. de Paula[1] and Daniel C. Nascimento[2]

1 CPqD - Telecommunications R&D Foundation, Brazil

2 ITA - Technological Institute of Aeronautics, Brazil

References

[1] Wong KL. Design of Nonplanar Microstrip Antennas and Transmission Lines. New York: John Wiley & Sons, Inc.; 1999.

[2] Josefsson L, Persson P. Conformal Array Antenna Theory and Design. Hoboken: John Wiley & Sons, Inc.; 2006.

[3] Vasylchenko A, Schols Y, De Raedt W, Vandenbosch GAE. Quality Assessment of Computational Techniques and Software Tools for Planar-Antenna Analysis. IEEE Antennas Propagat. Magazine 2009;51(1) 23–38.

[4] de Paula CB, Ferreira DB, Bianchi I. Algorithm for the Design of Linearly Polarised Microstrip Antennas. In: MOMAG 2012, 5-8 Aug. 2012, Joao Pessoa, Brazil. (in Portuguese)

[5] Pues H, de Capelle AV. Accurate Transmission-Line Model for the Rectangular Microstrip Antenna. IEE Proc.-H 1984;131(6) 334–340.

[6] Bhattacharyya AK, Shafai L, Gary R. Microstrip Antenna – A Generalized Transmission Line. Progress in Electromagnetics Research 1991; 4 45-84.

[7] Kishk AA. Analysis of Spherical Annular Microstrip Antennas. IEEE Trans. Antennas Propagat. 1993;41(3) 338–343.

[8] Richards WF, Lo YT, Harrison DD. An Improved Theory for Microstrip Antennas and Applications. IEEE Trans. Antennas Propagat. 1981;29(1) 38–46.

[9] Rahmat-Samii Y, Michielssen E. Electromagnetic Optimization by Genetic Algorithms. New York: Wiley; 1999.

[10] Maciel DCM. Circularly Polarised Microstrip Arrays for Beam Steering. MSc thesis. ITA – Technological Institute of Aeronautics; 2005. (in Portuguese)

[11] Hansen RC. Phased Array Antennas. New York: John Wiley & Sons; 1998.

[12] Tseng CY, Griffiths LJ. A Simple Algorithm to Achieve Desired Patterns for Arbitrary Arrays. IEEE Trans. on Signal Processing 1992;40(11) 2737–2746.

[13] Mathematica. Wolfram Research. http://www.wolfram.com/products/mathematica/ (accessed 15 June 2012).

[14] Nascimento DC, Lacava JCS. Design of Low-Cost Probe-Fed Microstrip Antennas. In: Nasimuddin N. (ed) Microstrip Antennas. Rijeka: InTech; 2011. p1-26.

[15] ADS. Agilent Technologies. http://www.agilent.com/find/eesof-ads/ (accessed 15 June 2012).

[16] Collin RE. Foundations for Microwave Engineering. 2nd ed. New York: McGraw-Hill; 1992.

[17] Ashkenazy J, Shtrikman S, Treves D. Electric Surface Current Model for the Analysis of Microstrip Antennas on Cylindrical Bodies. IEEE Trans. Antennas Propagat. 1985;33(3) 295-300.

[18] da Silva CM, Lumini F, Lacava JCS, Richards FP. Analysis of Cylindrical Arrays of Microstrip Rectangular Patches. Electron. Lett. 1991;27(9) 778-780.

[19] Tam WY, Luk KM. Far Field Analysis of Spherical-Circular Microstrip Antennas by Electric Surface Current Models. IEE Proc. H Microw., Antennas Propagat. 1991;138(1) 98-102.

[20] Sipus Z, Burum N, Skokic S, Kildal PS. Analysis of Spherical Arrays of Microstrip Antennas Using Moment Method in Spectral Domain. IEE Proc. Microw., Antennas and Propagat. 2006;153(6) 533-543.

[21] Tseng CY. Minimum Variance Beamforming with Phase-Independent Derivative Constraints. IEEE Trans. Antennas Propagat. 1992;40(3) 285–294.

[22] Allard RJ, Werner DH, Werner PL. Radiation Pattern Synthesis for Arrays of Conformal Antennas Mounted on Arbitrarily-Shaped Three-Dimensional Platforms Using Genetic Algorithms. IEEE Trans. Antennas Propagat. 2003;51(5) 1054-1062.

[23] Ferreira DB, de Paula CB, Nascimento DC. Design of an Active Feed Network for Antenna Arrays. In: MOMAG 2012, 5-8 Aug. 2012, Joao Pessoa, Brazil. (in Portuguese)

IntechOpen